ATOMIC PHYSICS

Creation of a Bose-condensed gas of ^{87}Rb by laser cooling

Jiazhong Hu,*† Alban Urvoy,* Zachary Vendeiro, Valentin Crépel, Wenlan Chen, Vladan Vuletić†

Protocols for attaining quantum degeneracy in atomic gases almost exclusively rely on evaporative cooling, a time-consuming final step associated with substantial atom loss. We demonstrate direct laser cooling of a gas of rubidium-87 (^{87}Rb) atoms to quantum degeneracy. The method is fast and induces little atom loss. The atoms are trapped in a two-dimensional optical lattice that enables cycles of compression to increase the density, followed by Raman sideband cooling to decrease the temperature. From a starting number of 2000 atoms, 1400 atoms reach quantum degeneracy in 300 milliseconds, as confirmed by a bimodal velocity distribution. The method should be broadly applicable to many bosonic and fermionic species and to systems where evaporative cooling is not possible.

The ability to prepare quantum-degenerate Bose (1–3) and Fermi (4) gases has opened a multitude of research areas, including quantum simulation of complex Hamiltonians (5) and of quantum phase transitions (6). Quantum-degenerate gases are prepared in two steps: fast laser cooling until a certain density and temperature limit are reached, followed by slower evaporative cooling to Bose-Einstein condensation (BEC) or below the Fermi temperature. Compared with laser cooling, evaporative cooling (1–4) is slower; in addition, it requires favorable atomic collision properties, and only a small fraction of the original ensemble is left at the end of the process. The one exception to the two-step scheme is strontium (7), which fea-

tures a very narrow optical transition. This enables the laser cooling of a thermal cloud in a large trap, while a small (1%) fraction of the ensemble undergoes BEC in a tighter, collisionally coupled trap. Previous attempts at laser cooling of other species, such as alkali atoms, stopped short of achieving BEC owing to two adverse effects that set in at high density: optical excitation of pairs of atoms at short distance, leading to light-induced loss (8, 9), and reabsorption of emitted photons at high optical density, leading to excess recoil heating (10).

With respect to reaching quantum degeneracy, laser cooling techniques can be characterized in terms of the phase space density $\mathcal{D}$, which is the peak occupation per quantum state for a thermal

cloud. Standard polarization gradient cooling (11) reaches $\mathcal{D} \sim 10^{-6}$. A considerable improvement is offered by Raman sideband cooling (RSC) (12–14), with which, by isolating the atoms from each other in a three-dimensional (3D) optical lattice, $\mathcal{D} \sim 10^{-2}$ has been reached (14). Demagnetization cooling of chromium has also reached $\mathcal{D} \sim 10^{-2}$ (15). A release-and-retrap compression approach (16) to increase the occupation in a 3D optical lattice attained, in combination with RSC, a record $\mathcal{D} \sim 0.03$ (17), limited by light-induced loss in doubly occupied lattice sites.

Here we show that by judicious choice of optical cooling parameters and trap geometry, it is possible to create a Bose condensate of ^{87}Rb atoms without any evaporation. Degenerate Raman sideband cooling (dRSC) (13) is performed with optical pumping light that is red-detuned by several hundred megahertz from the D_1 atomic transition. We use release-and-retrap compression (16, 17) to strongly increase the atomic density after each optical cooling cycle. Starting with 2000 atoms in the central trapping region, we reach quantum degeneracy in 300 ms with 1400 atoms, as observed through a bimodal velocity distribution.

The centerpiece of our setup is a square 2D optical lattice created by two orthogonal retroreflected beams, each with a power of 1.1 W and focused to an e^{-2} intensity waist of 18 µm at the
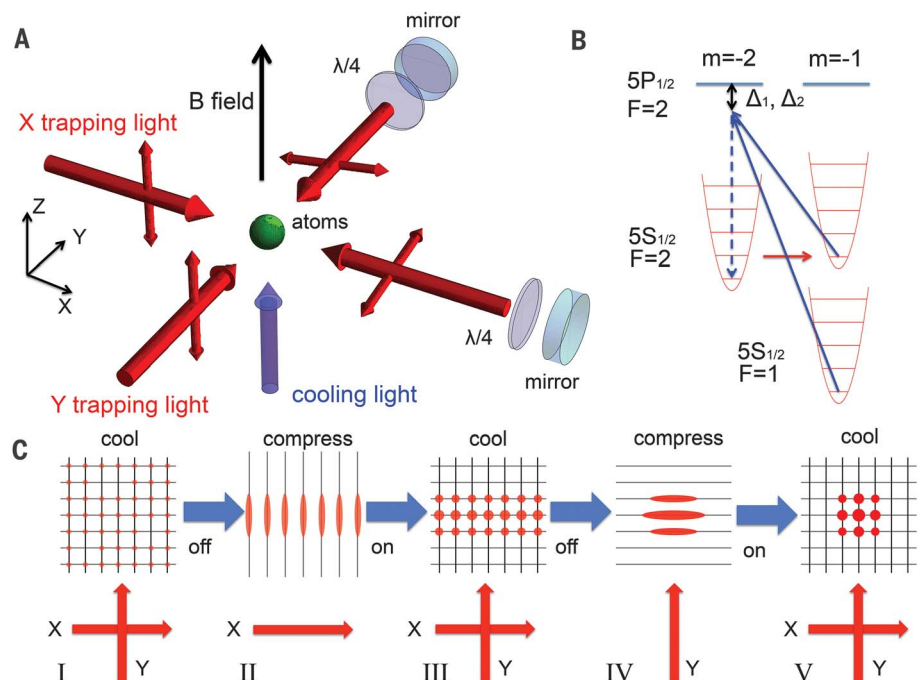
Department of Physics and Research Laboratory of Electronics, Massachusetts Institute of Technology, Cambridge, MA 02139, USA.
*These authors contributed equally to this work.
†Corresponding author. Email: jiazhong@mit.edu (J.H.); vuletic@mit.edu (V.V.)

Fig. 1. Experimental setup and procedure.
(**A**) ^{87}Rb atoms are trapped in a 2D lattice formed by two orthogonal retroreflected trapping beams at 1064 nm. The cooling light at 795 nm propagates along the magnetic field (z) and is σ^--polarized. (**B**) Simplified atomic-level structure for dRSC. The Zeeman splitting between two magnetic sublevels is matched to the vibrational splitting in the tightly confined direction. (**C**) Release-and-retrap compression sequence used to increase the atomic density. Starting from a sparsely filled 2D lattice, we perform dRSC (I) and then switch off the Y trapping beam to compress the atoms along y in the X trapping beam (II). After a short thermalization time, we switch back to the 2D lattice with an increased occupation number per trap (III). The procedure is repeated for the X beam to compress the atoms into a small number of tubes (IV). A final dRSC in this system (V) then yields a condensate.

atoms' position (Fig. 1). The incoming beams are vertically polarized, whereas the polarizations of the reflected beams are rotated by θ = 80°. This induces a polarization gradient in the lattice that provides the required Raman coupling for dRSC (13). The two retroreflected beams provide a trap depth of U/h = 13 MHz each (where h is Planck's constant), at an axial (tight) vibrational frequency of $\omega_{xy}/(2\pi)$ = 180 kHz and a radial vibration frequency along the vertical (z) direction of $\omega_z = \sqrt{2}\omega_{r2D} = 2\pi \times 6.3$ kHz. [Here, $\omega_{r2D}/(2\pi)$ = 4.5 kHz is the radial vibration frequency for a single 1D lattice beam.] A magnetic field B = 0.23 G along z is set to match the Zeeman splitting between the magnetic sublevels $|F = 2, m = -2\rangle$ and $|2, -1\rangle$ to $\hbar\omega_{xy}$ (where F is the total angular momentum; m, magnetic quantum number; $\hbar$, reduced Planck's constant).

A cooling cycle consists of a Raman transition $|2, -2\rangle \rightarrow |2, -1\rangle$ induced by the trapping light, which removes one vibrational quantum in the tightly confined direction (Fig. 1B), followed by optical pumping back to $|2, -2\rangle$. This reduces an atom's motional energy by $\sim \hbar\omega_{xy}$ per optical pumping cycle. The very-far-detuned trap light that drives the Raman transition (wavelength λ_t = 1064 nm) does not produce any appreciable atom loss, but the optical pumping can induce inelastic binary collisions as an atom pair is excited to a molecular potential that accelerates the atoms before they decay back to the ground state (9). To reduce this process relative to photon scattering by individual atoms (18), we use a σ⁻-polarized optical pumping beam tuned below the D_1 line away from photoassociation resonances (9, 15). Because an excited atom can also decay to F = 1, we use bichromatic light with detunings $\Delta_2/(2\pi)$ = –630 MHz and $\Delta_1/(2\pi)$ = –660 MHz relative to the $|5S_{1/2}, F = 2\rangle \rightarrow |5P_{1/2}, F' = 2\rangle$ and $|5S_{1/2}, F = 1\rangle \rightarrow |5P_{1/2}, F' = 2\rangle$ transitions, respectively. This far-detuned D_1-line optical pumping configuration reduces light-induced inelastic collisions by at least an order of magnitude.

The experimental sequence starts by accumulating ^{87}Rb atoms in a magneto-optical trap, loading them into the 2D lattice by means of polarization gradient cooling (16), and applying dRSC for 100 ms. This prepares the atoms near the vibrational ground state in the strongly confined x and y directions [the kinetic energy measured by time-of-flight imaging is K_{xy}/h = 50 kHz, close to $(\omega_{xy}/4)/(2\pi)$ = 45 kHz], whereas in the vertical direction (z), the atoms are cooled to $T_z \approx$ 12 μK (K_z/h = 120 kHz) through collisional thermalization between the axial and radial directions of the tubes. At this point, there are N = 2000 atoms in the 2D lattice with a peak occupation of $N_1 \approx 1$ atom per tube, corresponding to a peak phase space density $\mathcal{D}$ = 0.02 and peak density $n_0 = 2.2 \times 10^{14}$ cm⁻³. To further increase n_0 and $\mathcal{D}$, we apply release-and-retrap compression (16) by adiabatically turning off (in 400 μs) the Y trapping beam, so that the cloud shrinks in the y direction thanks to the radial confinement of the X trapping beam (Fig. 1C). After thermalization for 10 ms, the spatial extent of the cloud can

be estimated by $z = \sqrt{k_B T_z/m}/\omega_{r2D}$ = 1.1 μm, where T_z = 10 μK is the measured radial temperature, m is the ^{87}Rb mass, and k_B is Boltzmann's constant. The Y lattice beam is then turned back on in 1 ms. This loads the compressed ensemble back into a 2D lattice, resulting in a higher temperature ($T \sim 50$ μK), and we again apply dRSC for 100 ms. This yields again $K_{xy} \approx \hbar\omega_{xy}/4$ and T_z = 12 μK, but at a peak occupation number of N_1 = 6.9 atoms per tube, for a total number N = 1700 atoms. We repeat this procedure for the X lattice beam and end up with N = 1400 and N_1 = 47 at a peak density $n_0 = 1 \times 10^{16}$ cm⁻³. At this point, the ensemble is below our optical resolution of 8 μm, and N_1 is estimated from the measured temperatures in the corresponding 1D lattices and

the separately measured trap vibration frequencies. Figure 2D shows the evolution of N, N_1, and $\mathcal{D}$ during the sequence that brings the system close to $\mathcal{D} = 1$. We emphasize that evaporation is not occurring at any point because temperature reduction is only observed when the cooling light is on, and $k_B T \leq 0.1U$ at all times.

When we subsequently apply the final dRSC stage for up to 100 ms, we observe the gradual appearance of a characteristic signature of condensate formation: a bimodal distribution of the velocity along the z direction that becomes more pronounced with longer dRSC time t (Fig. 2). A fit to the observed distribution for t = 80 ms with a single Gaussian curve yields a reduced χ^2 = 137 (Fig. 2C), as opposed to χ^2 = 0.91 for a bimodal
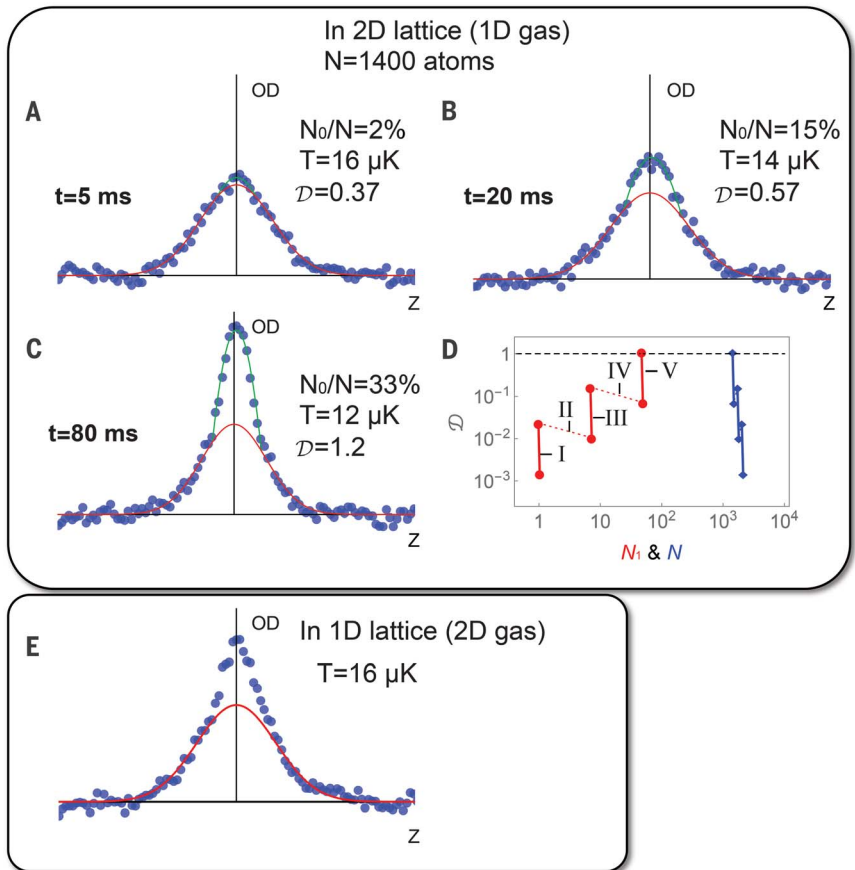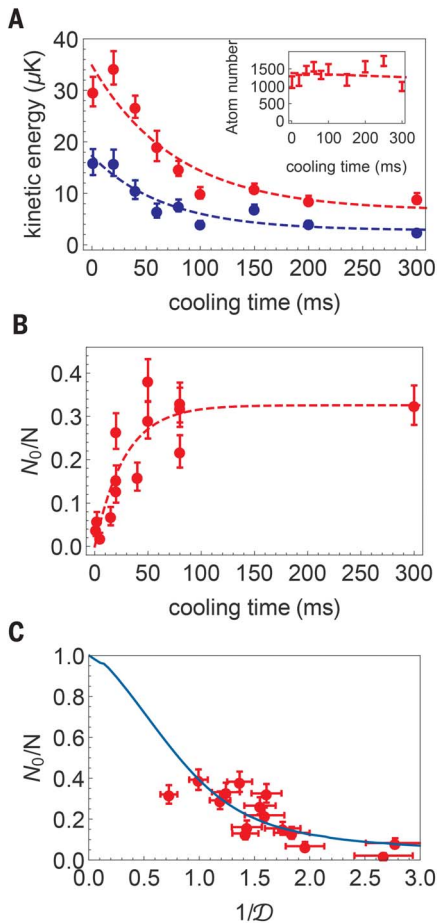

Fig. 2. Evidence of the formation of a Bose-condensed gas during optical cooling. A bimodal velocity distribution emerges during the final laser cooling stage, indicating macroscopic population of the ground state. (**A** to **C**) Observed optical depth (OD) along z after a ballistic expansion of 1.3 ms for cooling times of 5 ms (A), 20 ms (B), and 80 ms (C), averaged over 200 repetitions of the experiment. The red lines are Gaussian fits to the wings of the distributions, and green lines are quadratic fits to the remaining distribution in the center (19). Here the intensity of the trapping beams is ramped down in 400 μs—slowly compared with the axial trapping frequency but quickly with regard to the motion along z—to reduce the interaction energy. (**D**) Evolution of the total atom number N (blue) or atom number per lattice tube N_1 (red) versus the phase space density $\mathcal{D}$ during the sequence, with the steps labeled I to V as defined in Fig. 1B. The solid lines represent the dRSC process, and the dotted lines represent the spatial compression. Each cooling step enhances $\mathcal{D}$ by one order of magnitude, then the release-and-retrap compression increases the peak occupation number N_1 while slightly decreasing $\mathcal{D}$. (**E**) Velocity distribution along z for the same parameters as in (C), but observed for a 2D gas after releasing the atoms into the 1D lattice Y.

Fig. 3. Condensate fraction. (**A**) Cooling performance in the final stage. Average kinetic energy measured by the time-of-flight method in the directions of strong (blue) and weak (red) confinement is plotted against cooling time. After 80 ms of cooling, the atoms are in the 2D vibrational ground state. The inset shows that there is almost no atom loss during cooling. (**B**) Approximate condensate fraction versus cooling time, derived from the bimodal velocity distribution. In (A) and (B), the dashed lines are exponential fits. (**C**) Approximate condensate fraction versus the inverse peak phase space density $1/\mathcal{D}$. The blue line is a theoretical prediction for an ideal gas of 50 atoms in a 1D trap (*32*). Error bars, SEM.

distribution with a parabolic central component. (At $t = 5$ ms, the corresponding values are $\chi^2 = 0.89$ and $\chi^2 = 0.75$, respectively.) The bimodal distribution persists if we adiabatically turn off the X trap after cooling for $t = 80$ ms and observe the 2D gas in a 1D lattice (Fig. 2E).

In Fig. 3, we show the evolution of the kinetic energy, the bimodal distribution, and the atom number as a function of final-stage cooling time. Along the tightly confined directions, we cool to the vibrational ground state $K_{xy}/h = 50$ kHz $= 1.1 \times (\omega_{xy}/4)/(2\pi)$, whereas along z, we reach an aver-

age kinetic energy $K_z/h = 120$ kHz. Additionally, we observe only very limited atom loss (<5% at a peak density of $n_0 = 1 \times 10^{16}$ cm^{-3}; inset in Fig. 3A), confirming that light-induced losses are strongly suppressed. Figure 3C shows the condensate fraction N_0/N versus the calculated inverse phase space density $1/\mathcal{D}$ (*19*), where N_0 is the number of condensed atoms. In the absence of a detailed 1D theory, N_0/N is estimated as the fractional area under the narrower peak in the bimodal distribution. The onset of the bimodal distribution is observed near $\mathcal{D} = 0.7$. In 1D systems, only a smooth crossover to a quantum-degenerate gas occurs (*19–21*), which is in agreement with our observation for N_0/N. For our parameters, the system is in the crossover region between a weakly interacting 1D gas (*22*) and a strongly interacting Tonks-Girardeau gas (*23, 24*) (the calculated dimensionless interaction parameter is $\gamma \approx 2.7$ at the peak local density), as well as in the crossover region between a 1D Bose gas and a 3D finite-size condensate (*19, 25*). Although the character of the condensate is therefore ambiguous, the velocity distribution (Fig. 2) reveals a macroscopic population of the ground state.

Because the atomic cloud is below our optical resolution, the atomic density cannot be directly determined through optical imaging. However, an independent verification is possible by measuring three-body loss, where the loss coefficient [$K = 1.1 \times 10^{-28}$ cm^6 s^{-1} for a 3D thermal gas (*26*)] has been previously determined. In a 1D gas with $\gamma \approx 2.7$, the three-body loss is strongly suppressed by a factor of ~100 (*27, 28*), and indeed we do not detect any loss in the 1D tubes. Instead, we measure the three-body recombination in the 1D lattice (i.e., for a 2D gas), where we observe a lifetime of 300 ms; from this, we determine a peak density of 5.3×10^{14} cm^{-3} in the 2D gas, corresponding to a peak atom number of $N_1 \geq 45$ atoms per tube and a phase space density $\mathcal{D} = 1.1$ at the onset of quantum degeneracy (*19*), both in agreement with the previous estimation.

In our experiment, both the large red-detuning of the optical pumping light and the near-1D confinement observably reduce light-induced loss, whereas a photon-scattering rate below the trap vibration frequencies likely suppresses excess recoil heating in the festina lente regime (*10, 29*). Although there is no known simple relation between the momentum distribution and the condensate fraction in the crossover regime in which our experiment operates, we estimate that up to 40% of the ensemble, or 550 atoms, are in macroscopically occupied ground states of 30 tubes with a peak occupation of 50 atoms per tube.

We expect that the number of atoms in the condensate can be substantially increased in the future by using higher trap power and that the method can be applied to various bosonic and fermionic atomic species, potentially even under conditions where evaporative cooling is impossible. The far-detuned optical pumping light may also enable atom number–resolving measurements in quantum gas microscopes (*30, 31*). Last, the fast preparation may pave the way for

further studies of the strongly correlated Tonks gas regime (*23, 24*).

REFERENCES AND NOTES

1. M. H. Anderson, J. R. Ensher, M. R. Matthews, C. E. Wieman, E. A. Cornell, *Science* **269**, 198–201 (1995).
2. C. C. Bradley, C. A. Sackett, J. J. Tollett, R. G. Hulet, *Phys. Rev. Lett.* **75**, 1687–1690 (1995).
3. K. B. Davis *et al.*, *Phys. Rev. Lett.* **75**, 3969–3973 (1995).
4. B. DeMarco, D. S. Jin, *Science* **285**, 1703–1706 (1999).
5. I. Bloch, J. Dalibard, S. Nascimbene, *Nat. Phys.* **8**, 267–276 (2012).
6. K. W. Madison, F. Chevy, V. Bretin, J. Dalibard, *Phys. Rev. Lett.* **86**, 4443–4446 (2001).
7. S. Stellmer, B. Pasquiou, R. Grimm, F. Schreck, *Phys. Rev. Lett.* **110**, 263003 (2013).
8. T. Walker, P. Feng, *Adv. At. Mol. Opt. Phys.* **34**, 125–170 (1994).
9. K. Burnett, P. S. Julienne, K. Suominen, *Phys. Rev. Lett.* **77**, 1416–1419 (1996).
10. S. Wolf, S. J. Oliver, D. S. Weiss, *Phys. Rev. Lett.* **85**, 4249–4252 (2000).
11. J. Dalibard, C. Cohen-Tannoudji, *J. Opt. Soc. Am. B* **6**, 2023 (1989).
12. S. E. Hamann *et al.*, *Phys. Rev. Lett.* **80**, 4149–4152 (1998).
13. V. Vuletić, C. Chin, A. J. Kerman, S. Chu, *Phys. Rev. Lett.* **81**, 5768–5771 (1998).
14. A. J. Kerman, V. Vuletić, C. Chin, S. Chu, *Phys. Rev. Lett.* **84**, 439–442 (2000).
15. J. Rührig, T. Bäuerle, A. Griesmaier, T. Pfau, *Opt. Express* **23**, 5596–5606 (2015).
16. M. T. DePue, C. McCormick, S. L. Winoto, S. Oliver, D. S. Weiss, *Phys. Rev. Lett.* **82**, 2262–2265 (1999).
17. D.-J. Han *et al.*, *Phys. Rev. Lett.* **85**, 724–727 (2000).
18. V. Vuletić, C. Chin, A. J. Kerman, S. Chu, *Phys. Rev. Lett.* **83**, 943–946 (1999).
19. Supplementary materials.
20. D. S. Petrov, G. V. Shlyapnikov, J. T. M. Walraven, *Phys. Rev. Lett.* **85**, 3745–3749 (2000).
21. I. Bouchoule, K. V. Kheruntsyan, G. V. Shlyapnikov, *Phys. Rev. A* **75**, 031606 (2007).
22. P. Krüger, S. Hofferberth, I. E. Mazets, I. Lesanovsky, J. Schmiedmayer, *Phys. Rev. Lett.* **105**, 265302 (2010).
23. T. Kinoshita, T. Wenger, D. S. Weiss, *Science* **305**, 1125–1128 (2004).
24. B. Paredes *et al.*, *Nature* **429**, 277–281 (2004).
25. A. Görlitz *et al.*, *Phys. Rev. Lett.* **87**, 130402 (2001).
26. J. Söding *et al.*, *Appl. Phys. B* **69**, 257–261 (1999).
27. B. Laburthe Tolra *et al.*, *Phys. Rev. Lett.* **92**, 190401 (2004).
28. E. Haller *et al.*, *Phys. Rev. Lett.* **107**, 230404 (2011).
29. Y. Castin, J. I. Cirac, M. Lewenstein, *Phys. Rev. Lett.* **80**, 5305–5308 (1998).
30. W. S. Bakr, J. I. Gillen, A. Peng, S. Fölling, M. Greiner, *Nature* **462**, 74–77 (2009).
31. J. F. Sherson *et al.*, *Nature* **467**, 68–72 (2010).
32. W. Ketterle, N. J. van Druten, *Phys. Rev. A* **54**, 656–660 (1996).

SUPPLEMENTARY MATERIALS

www.sciencemag.org/content/358/6366/1078/suppl/DC1
Materials and Methods
Figs. S1 to S4
Table S1
References (*33, 34*)